Photoaffinity Labeling

International Edition: DOI: 10.1002/anie.201709584
German Edition: DOI: 10.1002/ange.201709584

Tetrazole-Based Probes for Integrated Phenotypic Screening, Affinity-Based Proteome Profiling, and Sensitive Detection of a Cancer Biomarker

Ke Cheng, Jun-Seok Lee, Piliang Hao, Shao Q. Yao, Ke Ding, and Zhengqiu Li**

Abstract: *Target-identification phenotypic screening has been a powerful approach in drug discovery; however, it is hindered by difficulties in identifying the underlying cellular targets. To address this challenge, we have combined phenotypic screening of a fully functionalized small-molecule library with competitive affinity-based proteome profiling to map and functionally characterize the targets of screening hits. Using this approach, we identified ANXA2, PDIA3/4, FLAD1, and NOS2 as primary cellular targets of two bioactive molecules that inhibit cancer cell proliferation. We further demonstrated that a panel of probes can label and/or image annexin A2 (a cancer biomarker) from different cancer cell lines, thus providing opportunities for potential cancer diagnosis and therapy.*

Phenotypic screening plays a pivotal role in the discovery of novel bioactive compounds.[1] However, the utility of phenotypic screening is limited by its difficulties in identifying the underlying cellular targets.[2] Common approaches for target identification, such as in vitro-based assays and affinity chromatography, mostly rely on recombinant proteins or crude cell lysates, rendering them unsuitable for reporting genuine drug–protein interactions in native environments.[3] To address these challenges, affinity-based proteome profiling (A*f*BP), in which photoprobes capable of recapitulating drug–protein interactions in situ leading to subsequent protein enrichment and large-scale proteome-wide target identification, has been developed as a powerful approach for in situ target identification during the past decade.[4] In order to further improve this approach, we have developed three types of minimalist bioorthogonal handle-containing photo-crosslinkers (**L3–6**) capable of facilitating the synthesis of affinity-based probes (A*f*BPs) and enabling simultaneous proteome profiling and live-cell imaging.[5]

As a widely applied approach for target identification, A*f*BP still suffers from two key issues, nonspecific labeling and unsatisfactory photo-crosslinking yield.[6] To alleviate these issues, competitive proteome profiling is usually employed to distinguish between background labeling and specific crosslinking.[7] On the other hand, several groups have comprehensively studied the background inventory of different photo-crosslinkers, which can help to eliminate non-specifically labeled proteins from target candidates.[8] Moreover, we have recently developed novel diaryltetrazole-based photo-crosslinkers, which possess superior photo-crosslinking efficiency and one-/two-photon fluorescence turn-on properties, and are suitable for simultaneous in situ proteome profiling and no-wash real-time imaging.[9] Owing to their unique crosslinking mechanism (Figure 1 A), the photo-induced nitrile imines generated from these photo-crosslinkers are capable of undergoing rapid reactions with a variety of biological nucleophiles (that is, acids, thiols, and amines) and electrophiles (that is, electron-deficient alkenes) but have shown preferential labeling of proteins at their aspartic acid (Asp) and glutamic acid (Glu) residues with reduced photo-crosslinker-associated nonspecific background

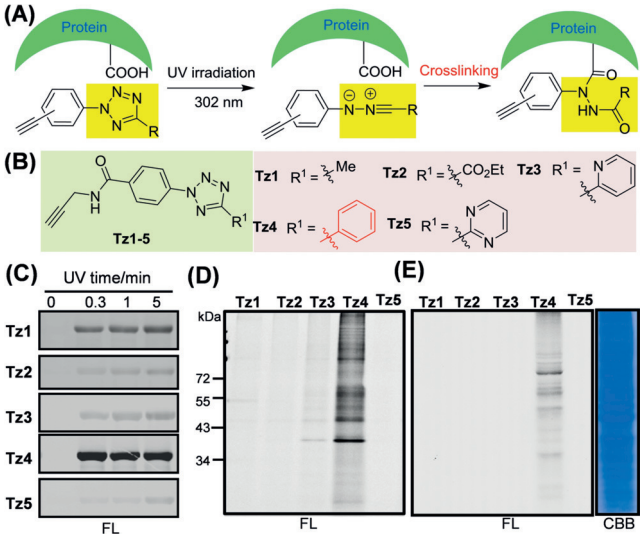

Figure 1. A) The carboxylate-selective photo-crosslinking mechanism between a tetrazole and a protein. B) Structures of compounds **Tz1–5**. C) Time-dependent labeling of BSA (2 μg) with **Tz1–5** (1 μM) in PBS buffer. Proteome reactivity profiles of D) cell lysates and E) live MCF-7 cells treated with **Tz1–5**. FL = in-gel fluorescence scanning. CBB = Coomassie brilliant blue gel.

[*] K. Cheng, Prof. K. Ding, Prof. Z. Li
School of Pharmacy, Jinan University
601 Huangpu Avenue West, Guangzhou, 510632 (China)
E-mail: dingke@jnu.edu.cn
pharmlzq@jnu.edu.cn
Prof. S. Q. Yao
Department of Chemistry
National University of Singapore (Singapore)
Prof. J.-S. Lee
Molecular Recognition Research Center, Korea Institute of Science and Technology (KIST), and Department of Biological Chemistry, University of Science & Technology (Republic of Korea)
Prof. P. Hao
School of Life Science and Technology, ShanghaiTech University (China)
Supporting information and the ORCID identification number(s) for the author(s) of this article can be found under: https://doi.org/10.1002/anie.201709584.

labeling. Despite their frequent occurrence in a protein (>12% with combined proportion of Asp and Glu),[10] few carboxylate-selective protein-labeling reactions are currently available.[11] Our findings were further confirmed by a follow-up work from Lin's group, which showed 2-aryl-5-carboxytetrazole (ACT) can serve as an excellent photo-crosslinker in A*f*BP studies.[12]

Recently, Cravatt et al. reported that phenotypic screening and target identification can be integrated by using affinity-based probe compound libraries, so as to accelerate the mechanistic characterization of screening hits.[13] Inspired by these elegant strategies, we endeavored to incorporate a diaryltetrazole, a group that can simultaneously act as a photo-crosslinker and a bioactive moiety, and an alkyne handle into a 20-membered small-molecule library, with the aim to discover bioactive tetrazole-based molecules followed by the identification of the interacting cellular targets.

Given that the effects of different substituents on the photolysis of tetrazole have not been well studied, we synthesized five probes (**Tz1**–**5**) bearing methyl, ester, phenyl, 2-pyridyl, and 2-pyrimidyl groups at the 5-position, following the typical synthetic methods of tetrazoles (Figure 1B and the Supporting Information, Schemes S1 and S2);[14] an alkyne handle was embedded into the probes for visualization, enrichment, and identification of interacting proteins. We first evaluated the rate of photolysis of **Tz1**–**5** by HPLC analysis (Supporting Information, Figure S1); upon exposure of each of the probes (dissolved in PBS buffer) to 302 nm UV light for different periods of time followed by HPLC separation of the reaction products, complete photolysis of **Tz1** and **Tz2** was observed within 5 and 2 min, respectively, indicating that the electron-withdrawing ester group in **Tz2** was beneficial for the photolysis. Interestingly, **Tz3**–**5** appeared to be more efficient than **Tz1** and **Tz2** and their complete photolysis could be observed in as little as 1 min. Next, time-dependent labeling with bovine serum albumin (BSA) was carried out to assess the photo-crosslinking ability of these probes. Upon incubation of BSA with each of the probes for 10 min in PBS buffer, the resulting mixtures were exposed to UV light (302 nm) for different periods of time, clicked with TAMRA-N_3 and separated by SDS-PAGE. Fluorescently labeled BSA was finally visualized and quantified by in-gel fluorescence scanning (Figure 1C); we observed strong fluorescent bands of **Tz4**/BSA labeling in as little as 20 s with 1 μM of the probe. On the contrary, the labeling profiles of **Tz1**–**3** and **Tz5** appeared to be significantly weaker under the same labeling conditions across all irradiation times. Furthermore, we carried out labeling profiles of MCF-7 lysates with **Tz1**–**5** under the same labeling conditions as the BSA labeling, which also showed that only **Tz4**-treated sample showed notable labeling bands (Figure 1D, lane 4). These results indicate that 2,5-diphenyltetrazole (**Tz4**) is an efficient photo-crosslinker with superior protein crosslinking ability. Encouraged by the excellent in vitro crosslinking efficiency of **Tz4**, we sought to assess its in situ labeling properties. Upon incubation of **Tz1**–**5** with live MCF-7 cells for 5 h, the cells were irradiated with UV light and then lysed; the resulting cell lysates were conjugated with TAMRA-N_3 and separated by SDS-PAGE followed by in-gel fluorescence scanning (Figure 1E). Only **Tz4**-treated samples showed fluorescently labeled bands, highlighting the efficient labeling ability of 2,5-diphenyltetrazole in situ. To identify the cross-linked targets in cell lysates and live cells, labeled proteins under both settings were clicked with TAMRA-Biotin-N_3 and then enriched using avidin–agarose beads, separated on SDS-PAGE, followed by LC-MS/MS analysis. As listed in the Supporting Information, Table S1, a series of high-abundance proteins, such as CD9, CD44, PRC1, and CC2D1A, were positively identified. Compared with previously reported background inventory of three common photo-crosslinkers (diazirine, benzophenone, and arylazide),[8] the background proteins of diaryltetrazole include unique and common proteins, which can be useful references for A*f*BP, especially in cases in which diaryltetrazole is chosen as a photo-crosslinker in the probe design.

After confirming that 2,5-diphenyltetrazole is an efficient photo-crosslinker under both in vitro and in situ settings, we next set out to prepare a photoprobe library by incorporating different substituents at the 2- and 5-positions (**Tz6**–**20**, Figure 2A). The synthesis was largely based on published methods (Supporting Information, Scheme S3–6). Two non-clickable analogues of **Tz6** and **Tz10**, **Tz21** and **Tz22**, were prepared accordingly as competitors (Supporting Information, Scheme S7). With these probes in hand, we first evaluated the labeling performance of the library in mammalian cells (5 μM final probe concentration, 10 min of UV irradiation). As shown in Figure 2B, individual probes showed markedly distinct protein-labeling profiles, which indicates the diverse elements introduced into the probe library were sufficient to direct the preferential binding of different probes to various sub-proteomes in the cells. Interestingly, these in situ proteome reactivity profiles were different from the corresponding profiles obtained under in vitro conditions (Supporting Information, Figure S3A), indicating that the probes interacted with different sets of proteins between live cells and cell lysates.

Subsequently, we tested the inhibitory activities of the probe library against three common cancer cell lines (MCF-7, HepG2, and MDA-MB-231; Figure 2C,D and the Supporting Information, Figure S2). Gratifyingly, two probes, **Tz6** and **Tz10**, exhibited potent antiproliferative effects under normal cell culture conditions with IC_{50} values of 4.1 and 0.69 μM, respectively. Remarkably, the cytotoxicity of **Tz10** was comparable to that of doxorubicin (a well-known anticancer drug). The corresponding alkyne handle-free competitors, **Tz21** and **Tz22**, displayed comparable antiproliferative activities in MCF-7 cells (Figure 2C,D). We found that the structures of **Tz6** and **Tz10** differ from the other molecules only in the amide moiety, suggesting that this part is essential for maintaining the compounds' observed bioactivities. Similar to previously reported bioactive molecules,[13a] probes bearing a *t*-butoxycarbamoylpiperazine carbonyl group (that is, **Tz6**, **Tz9**, and **Tz14**) also exhibited moderate antiproliferative effects in MCF-7 cells (Figure 2C).

To identify the cellular targets of the two most potent probes, **Tz6** and **Tz10**, chemoproteomic experiments and live-cell bioimaging were next carried out concurrently. As shown in Figure 3A, the in situ proteome labeling was performed by

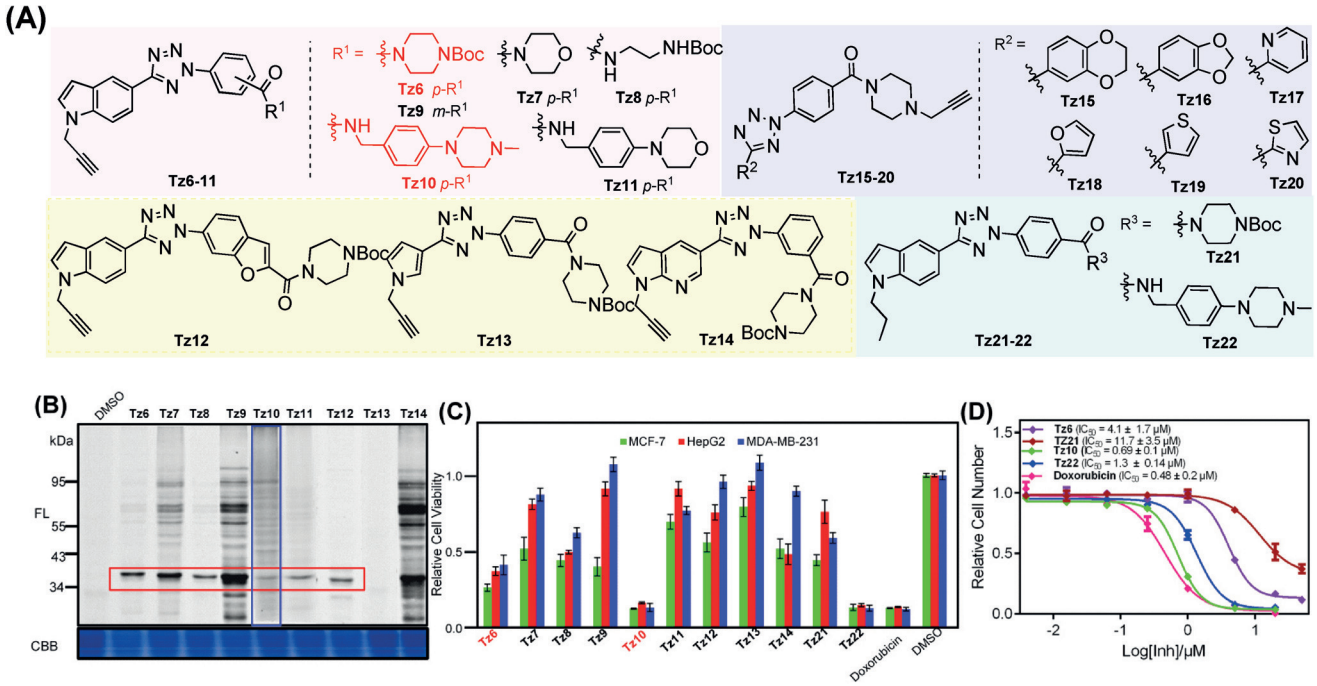

Figure 2. A) Structures of the probes **Tz6–22** (red-colored probes were used in the following biological studies). B) Proteome reactivity profiles of live MCF-7 cells treated with **Tz6–14** (5 μM final concentration, 10 min of UV irradiation). C) Inhibition of cancer cell viability of **Tz6—22** determined by CCK8 assay. D) IC_{50} values of **Tz6**, **Tz10**, **Tz21**, and **Tz22** against MCF-7 cells.

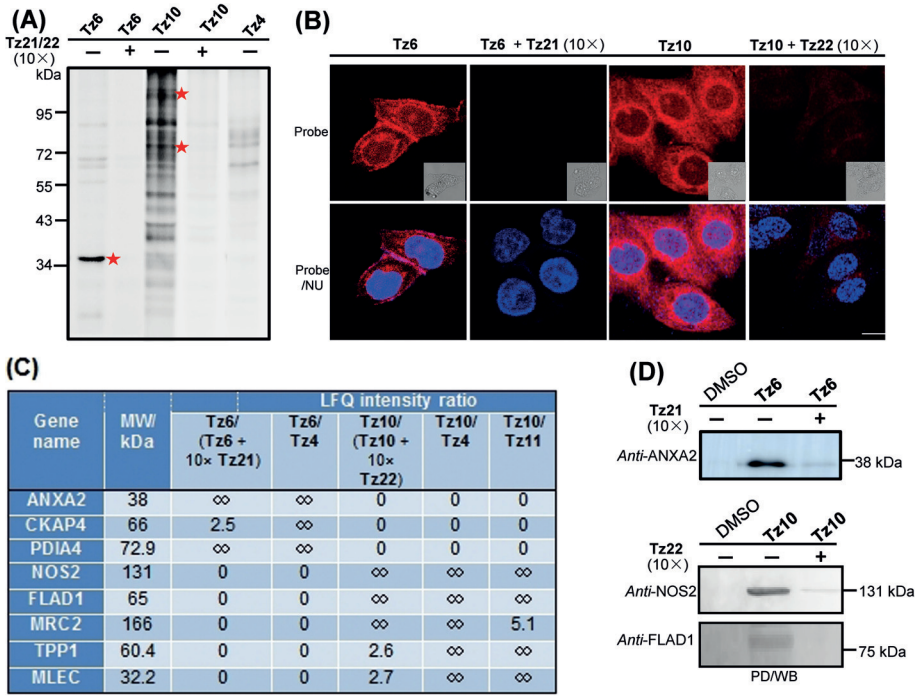

Gene name	MW/ kDa	LFQ intensity ratio				
		Tz6/ (Tz6 + 10× Tz21)	Tz6/ Tz4	Tz10/ (Tz10 + 10× Tz22)	Tz10/ Tz4	Tz10/ Tz11
ANXA2	38	∞	∞	0	0	0
CKAP4	66	2.5	∞	0	0	0
PDIA4	72.9	∞	∞	0	0	0
NOS2	131	0	0	∞	∞	∞
FLAD1	65	0	0	∞	∞	∞
MRC2	166	0	0	∞	∞	5.1
TPP1	60.4	0	0	2.6	∞	∞
MLEC	32.2	0	0	2.7	∞	∞

Figure 3. A) Proteome reactivity profiles of live MCF-7 cells treated with **Tz4**, **Tz6**, and **Tz10** in the presence or absence of corresponding competitors (2 μM final concentration, 10 min of UV irradiation). B) Live-cell imaging of MCF-7 cells with **Tz6**/**10** (2 μM) in the presence or absence of corresponding competitors. Scale bar = 10 μm. C) High-confidence protein hits of **Tz6** and **Tz10**, "∞" means infinity, "0" means not appearing. D) Validation of three protein hits by pull-down/WB. WB = western blotting.

following the procedures described above with the inactive **Tz4** probe as a control (lane 5) but at a lower probe concentration (2 μM) in order to reduce nonspecific binding. As shown in Figure 3 A, while the **Tz4**-treated sample showed an overall negligible nonspecific labeling profile (lane 5), which again confirmed the low background labeling property of tetrazole photo-crosslinkers in general as earlier discussed (for example, Figure 1), the **Tz6**-treated sample showed a highly selective probe labeling profile, with a strong fluorescently labeled band predominantly at circa 37 kDa and several much fainter bands at circa 72 kDa (lane 1), indicating excellent target selectivity. In the presence of excess **Tz21** (10×) as a competitor, all fluorescent bands including the 37-kDa band were abolished (lane 2), indicating they were potential **Tz21**-targeted proteins and not background proteins caused by nonspecific photo-crosslinking. In sharp contrast, the **Tz10**-treated sample showed a significantly less selective, albeit still **Tz22**-competitive, probe labeling profile, resulting in strong fluorescently labeled bands throughout the whole lane (lane 3). To track the subcellular probe localization, cellular imaging of

live MCF-7 cells with **Tz6** and **Tz10** was next carried out. The cells were first treated with each probe followed by UV irradiation to initiate photo-crosslinking. Subsequently, cells were fixed, permeabilized, and clicked with TAMRA-N_3 under previously optimized click chemistry conditions,[5b,c,9] then imaged. Strong fluorescence signals were observed in the cell membrane and nucleus from **Tz6**-treated cells, while **Tz10** mainly located outside of the nucleus. Consistently, the fluorescence signals of both probes were abolished in the presence of excess competitors (Figure 3B). Control imaging experiments with DMSO under similar conditions gave minimal background fluorescence compared to labeled cells (Supporting Information, Figure S5). Results from these competitive in situ labeling and live-cell imaging experiments thus indicate that both **Tz6** and **T10** were able to efficiently capture their intended cellular targets, and **Tz6** appeared to have highly selective cellular targets.

We next proceeded to identify potential cellular targets of **Tz6** and **Tz10** by large-scale chemoproteomics experiments. Similar to the procedures described above, probe-labeled proteins were affinity-purified and identified by LC-MS/MS analysis following in situ proteome labeling and click chemistry with TAMAR-Biotin-N_3. Control experiments were done concurrently with DMSO- and **Tz4**-treated control samples, which served to filter out false hits identified from the LC-MS/MS experiments as a result of background photo-crosslinking and/or nonspecific protein binding. In addition, only proteins that appeared in duplicated runs and whose LFQ intensity[15] ratios from probe-treated and competitive labeling experiments (that is, **Tz6** vs. [**Tz6** + **Tz21**(10×)], or **Tz10** vs. [**Tz10** + **Tz22**(10×)]) of greater than 2 were considered further. Finally, a comparison of the proteomic targets of **Tz10** versus **Tz11**, an inactive analogue differs only in the position of piperidine, was made to reveal proteins relevant for antiproliferative activity of **Tz10** (LFQ ratio > 2). As listed in Figure 3C and the Supporting Information, Tables S3 and S4, 35 and 60 protein hits met these criteria for **Tz6** and **Tz10**, respectively. Further analysis of these protein hits revealed that annexin A2 (ANXA2) could match the circa 37-kDa major band detected in **Tz6**-labeled proteomes (Figure 3A, * in lane 1), while flavin adenine dinucleotide synthetase 1 (FLAD1) and nitric oxide synthase (NOS2) could match the labeling bands at circa 70 kDa and circa 130 kDa, respectively, in **Tz10**-treated sample (Figure 3A, * in lane 3). These three target candidates were further validated by pull-down/western blotting (WB) with the corresponding antibodies (Figure 3D). Moreover, we found that the locations of most proteins hits coincided well with the imaging results (Figure 3B);[16] for example, the protein hits of **Tz6**, ANXA2, VDAC, and CKAP4, are known to be mainly located in the cell membrane, and the **Tz10**-identified proteins NOS2 and FLAD1 are predominantly cytosolic proteins. We further verified ANXA2 and NOS2 by immunofluorescence experiments, following our previous protocols (Supporting Information, Figure S5).[5b,c] These lines of evidence underscored the high reliability of these protein hits, and it is possible that **Tz6** and **Tz10** produce their antiproliferative effects through a combination of these protein targets.

Considering annexin A2 is a cancer biomarker,[17] it is of great importance to develop suitable small molecule probes that can detect its cellular expression/activity in situ. Herein, we further evaluated the labeling sensitivity of **Tz6** and other probes toward annexin A2 by concentration- and time-dependent labeling experiments. As shown in Figure 4A,

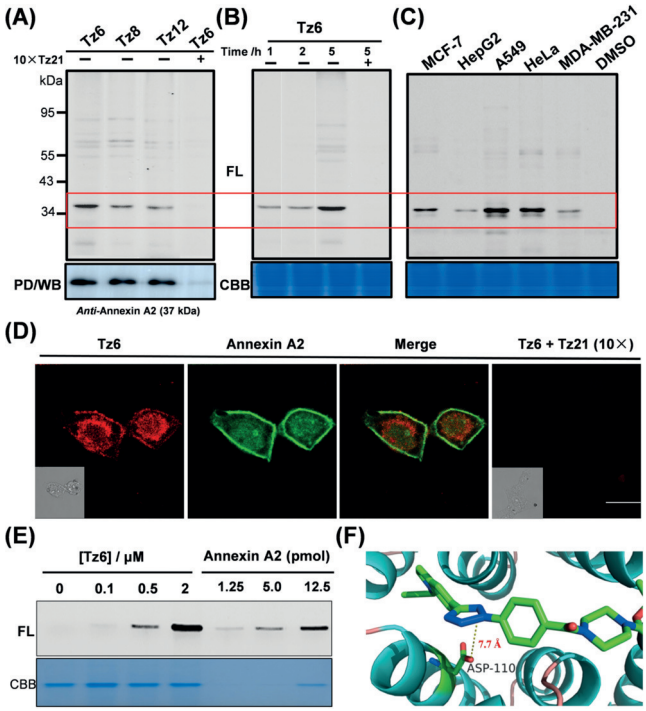

Figure 4. A) Labeling profiles of MCF-7 cells with **Tz6, Tz8**, and **Tz12** (2 μM), in the presence or absence of competitor (**Tz21**). The corresponding pull-down/western blot (WB) are shown (bottom gel). B) Time-dependent in situ labeling with **Tz6** (2 μM). C) Labeling profiles of different cancer cell lines with **Tz6** (2 μM). D) Live-cell imaging of MCF-7 cells with **Tz6** (2 μM). Immunofluorescence (IF) staining using anti-annexin A2 antibodies. Scale bar = 10 μm. E) Labeling of recombinant annexin A2 protein with **Tz6** (different concentrations of **Tz6** or different amount of protein). F) ASP-110, the binding site of **Tz6** with annexin A2 identified by LC-MS/MS and docking experiments to predict the binding mode of **Tz6** with annexin A2.

Tz6, **Tz8**, and **Tz12** can successfully label ANXA2 at a probe concentration of 2 μM, which was confirmed by pull-down/WB (Figure 4A, bottom gel). An even lower concentration of the probes (1 μM) was sufficient to produce prominent corresponding bands in live MCF-7 cells from concentration-dependent labeling experiments (Figure S3C). Time-dependent labeling experiments revealed that the circa 37 kDa band was visible within 1 h (Figure 4B). Importantly with **Tz6**, the highly selective ANXA2 labeling profiles could be successfully recapitulated in various cancer cell lines, including HepG2, A549, HeLa and MDA-MB-231 (Figure 4C), suggesting that this probe has the potential of broad applications in detecting endogenous ANXA2. It is also noteworthy that, from the immunofluorescence (IF) experiments performed with anti-ANXA2, the resulting fluorescence signals appeared to overlap well with those obtained from staining the same cells with **Tz6** (Figure 4D and

Figure S5), implying that **Tz6** can report this protein's activities by both protein labeling and live-cell imaging experiments. In addition, labeling experiments of recombinant annexin A2 with **Tz6** revealed that the protein could be successfully labeled by the probe at probe concentrations as low as 0.5 μM with 1 μg of the protein, and as little as 1.25 pmol of the protein could be successfully detected by **Tz6** at 1 μM (Figure 4E), showing that this probe possesses excellent sensitivity toward annexin A2. To map the potential labeling sites of **Tz6** in annexin A2, the probe-labeled recombinant protein was analyzed by LC-MS/MS. Asp^{110}, a residue located in the active region of the protein was positively identified (Figure 4F and the Supporting Information, Figure S6).[18] This crosslinking pattern is consistent with the results previously reported by us and others.[9,12] Docking experiments revealed that the distance between the tetrazole in **Tz6** and Asp^{110} was around 7.7 Å, which is a reasonable distance for successful photo-crosslinking. Finally, we evaluated the photo-crosslinking efficiency of **Tz6** with recombinant annexin A2 by pull-down/WB, which appeared to be very high (Supporting Information, Figure S7).

In conclusion, we demonstrated that 2,5-diphenyltetrazole can display superior photo-crosslinking efficiency under both in vitro and in situ settings. Diaryltetrazole-based probes bearing an alkyne handle were suitable for integrated phenotypic screening and target identification. We identified the cellular targets of two hit compounds, **Tz6** and **Tz10**, by affinity-based proteome profiling coupled with live-cell bioimaging. Most protein hits are disease-related targets. Importantly, several probes from our current study, especially **Tz6**, were able to label endogenous annexin A2 with excellent selectivity and sensitivity under highly complex native cellular environments from different mammalian cells. With these outstanding properties, we expect that these novel small molecule probes could find potential applications in cancer-related diagnoses and therapy.

Acknowledgements

Funding was provided by National Natural Science Foundation of China (21602079), Science and Technology Program of Guangdong province (2017A050506028), Science and Technology Program of Guangzhou (201704030060), KIST (2E26632/2E26110, CAP- 16-02-KIST) and the Bio & Medical Technology Development Program of the National Research Foundation (NRF- 2016M3A9B6902060, NRF-2017M3A9D8029942) from Ministry of Science, Korea. We thank Dr. W. Lorenzo (JNU) and Dr. L. Gao (IBN) for the invaluable suggestions on this work.

Conflict of interest

The authors declare no conflict of interest.

Keywords: affinity-based probes · cancer biomarkers · phenotypic screening · target identification · tetrazole

How to cite: *Angew. Chem. Int. Ed.* **2017**, *56*, 15044–15048
Angew. Chem. **2017**, *129*, 15240–15244

[1] a) J. G. Moffat, J. Rudolph, D. Bailey, *Nat. Rev. Drug Discovery* **2014**, *13*, 588–602; b) S. J. Warchal, A. Unciti-Broceta, N. O. Carragher, *Future Med. Chem.* **2016**, *8*, 1331–1347.
[2] E. Dominguez, A. Galmozzi, J. W. Chang, K. L. Hsu, J. Pawlak, W. Li, C. Godio, J. Thomas, D. Partida, S. Niessen, P. E. O'Brien, A. P. Russell, M. J. Watt, D. K. Nomura, B. F. Cravatt, E. Saez, *Nat. Chem. Biol.* **2014**, *10*, 113–121.
[3] a) T. Anastassiadis, S. W. Deacon, K. Devarajan, H. Ma, J. R. Peterson, *Nat. Biotechnol.* **2011**, *29*, 1039–1045; b) M. Bantscheff, D. Eberhard, Y. Abraham, S. Bastuck, et al., *Nat. Biotechnol.* **2007**, *25*, 1035–1044.
[4] a) S. Pan, H. Zhang, C. Wang, S. C. Yao, S. Q. Yao, *Nat. Prod. Rep.* **2016**, *4*, 612–620; b) J. Sumranjit, S. J. Chung, *Molecules* **2013**, *18*, 10425–10451.
[5] a) H. Guo, Z. Li, *MedChemComm* **2017**, *8*, 1585–1591; b) Z. Li, P. Hao, L. Li, C. Y. J. Tan, X. Cheng, G. Y. J. Chen, S. K. Sze, H.-M. Shen, S. Q. Yao, *Angew. Chem. Int. Ed.* **2013**, *52*, 8551–8556; *Angew. Chem.* **2013**, *125*, 8713–8718; c) Z. Li, D. Wang, L. Li, S. Pan, Z. Na, C. Y. J. Tan, S. Q. Yao, *J. Am. Chem. Soc.* **2014**, *136*, 9990–9998.
[6] E. Smith, I. Collins, *Future Med. Chem.* **2015**, *7*, 159–183.
[7] H. Guo, J. Xu, P. Hao, K. Ding, Z. Li, *Chem. Commun.* **2017**, *53*, 9620–9623.
[8] a) J. Park, M. Koh, J. Y. Koo, S. Lee, S. B. Park, *ACS Chem. Biol.* **2016**, *11*, 44–52; b) H. Park, J. Y. Koo, Y. V. Srikanth, S. Oh, J. Lee, J. Park, S. B. Park, *Chem. Commun.* **2016**, *52*, 5828–5831; c) P. Kleiner, W. Heydenreuter, M. Stahl, V. S. Korotkov, S. A. Sieber, *Angew. Chem. Int. Ed.* **2017**, *56*, 1396–1401; *Angew. Chem.* **2017**, *129*, 1417–1422.
[9] Z. Li, L. Qian, L. Li, J. C. Bernhammer, H. V. Huynh, J. S. Lee, S. Q. Yao, *Angew. Chem. Int. Ed.* **2016**, *55*, 2002–2006; *Angew. Chem.* **2016**, *128*, 2042–2046.
[10] S. Yoshikawa, T. Tanimura, A. Miyawaki, M. Nakamura, M. Yuzaki, T. Furuichi, K. Mikoshiba, *J. Biol. Chem.* **1992**, *267*, 16613–16619.
[11] L. Leder, *Methods Mol. Biol.* **2015**, *1266*, 7–27.
[12] A. Herner, J. Marjanovic, T. M. Lewandowski, V. Marin, M. Patterson, L. Miesbauer, D. Ready, J. Williams, A. Vasudevan, Q. Lin, *J. Am. Chem. Soc.* **2016**, *138*, 14609–14615.
[13] a) J. S. Cisar, B. F. Cravatt, *J. Am. Chem. Soc.* **2012**, *134*, 10385–10388; b) T. Kambe, B. E. Correia, M. J. Niphakis, B. F. Cravatt, *J. Am. Chem. Soc.* **2014**, *136*, 10777–10782; c) C. G. Parker, A. Galmozzi, Y. Wang, B. E. Correia, K. Sasaki, C. M. Joslyn, A. S. Kim, C. L. Cavallaro, R. M. Lawrence, S. R. Johnson, I. Narvaiza, E. Saez, B. F. Cravatt, *Cell* **2017**, *168*, 527–541.
[14] Y. Wang, W. Song, W. J. Hu, Q. Lin, *Angew. Chem. Int. Ed.* **2009**, *48*, 5330–5333; *Angew. Chem.* **2009**, *121*, 5434–5437.
[15] J. Cox, M. Y. Hein, C. A. Luber, I. Paron, N. Nagaraj, M. Mann, *Mol. Cell. Proteomics* **2014**, *13*, 2513–2526.
[16] The information about the protein locations was obtained from the Genecards database (http://www.genecards.org/).
[17] a) F. Tas, C. Tilgen Yasasever, S. Karabulut, D. Tastekin, D. Duranyildiz, *Biomed. Pharmacother.* **2015**, *69*, 237–241; b) Y. R. Jeon, S. Y. Kim, E. J. Lee, Y. N. Kim, D. Y. Noh, S. Y. Park, A. Moon, *Proteomics* **2013**, *13*, 3145–3156.
[18] Y. Liu, H. K. Myrvang, L. V. Dekker, *Br. J. Pharmacol.* **2015**, *172*, 1664–1676.

Manuscript received: September 16, 2017
Accepted manuscript online: October 1, 2017
Version of record online: October 23, 2017

